Since January 2020 Elsevier has created a COVID-19 resource centre with free information in English and Mandarin on the novel coronavirus COVID-19. The COVID-19 resource centre is hosted on Elsevier Connect, the company's public news and information website.

Phytomedicine 85 (2021) 153310

Contents lists available at ScienceDirect

Phytomedicine

journal homepage: www.elsevier.com/locate/phymed

Original Article

Caffeic acid derivatives (CAFDs) as inhibitors of SARS-CoV-2: CAFDs-based functional foods as a potential alternative approach to combat COVID-19

Şevki Adem [a], Volkan Eyupoglu [a], Iqra Sarfraz [b], Azhar Rasul [b,*], Ameer Fawad Zahoor [c], Muhammad Ali [d], Mohnad Abdalla [e], Ibrahim M Ibrahim [f], Abdo A Elfiky [f]

[a] Department of Chemistry, Faculty of Sciences, Çankırı Karatekin University, 18100 Çankırı, Turkey
[b] Cell and Molecular Biology Lab, Department of Zoology, Faculty of Life Sciences, Government College University Faisalabad, 38000 Faisalabad, Pakistan
[c] Department of Chemistry, Faculty of Life Sciences, Government College University Faisalabad, 38000 Faisalabad, Pakistan
[d] Vice Chancellor, Quaid-e-Azam University (QAU), Islamabad
[e] Key Laboratory of Chemical Biology (Ministry of Education), Department of Pharmaceutics, School of Pharmaceutical Sciences, Cheeloo College of Medicine, Shandong University, 44 Cultural West Road, Shandong Province 250012, PR China
[f] Biophysics Department, Faculty of Sciences, Cairo University, Giza, 12613, Egypt

ARTICLE INFO

Keywords:
COVID-19
SARS-CoV-2
Bioactive phytochemicals
Caffeic acid derivative

ABSTRACT

Background: SARS-CoV-2, an emerging strain of coronavirus, has affected millions of people from all the continents of world and received worldwide attention. This emerging health crisis calls for the urgent development of specific therapeutics against COVID-19 to potentially reduce the burden of this emerging pandemic.
Purpose: This study aims to evaluate the anti-viral efficacy of natural bioactive entities against COVID-19 via molecular docking and molecular dynamics simulation.
Methods: A library of 27 caffeic-acid derivatives was screened against 5 proteins of SARS-CoV-2 by using Molegro Virtual Docker 7 to obtain the binding energies and interactions between compounds and SARS-CoV-2 proteins. ADME properties and toxicity profiles were investigated via www.swissadme.ch web tools and Toxtree respectively. Molecular dynamics simulation was performed to determine the stability of the lead-protein interactions.
Results: Our obtained results has uncovered khainaoside C, 6-O-Caffeoylarbutin, khainaoside B, khainaoside C and vitexfolin A as potent modulators of COVID-19 possessing more binding energies than nelfinavir against COVID-19 M^{pro}, Nsp15, SARS-CoV-2 spike S2 subunit, spike open state and closed state structure respectively. While Calceolarioside B was identified as pan inhibitor, showing strong molecular interactions with all proteins except SARS-CoV-2 spike glycoprotein closed state. The results are supported by 20 ns molecular dynamics simulations of the best complexes.
Conclusion: This study will hopefully pave a way for development of phytonutrients-based antiviral therapeutic for treatment or prevention of COVID-19 and further studies are recommended to evaluate the antiviral effects of these phytochemicals against SARS-CoV-2 in *in vitro* and *in vivo* models.

Introduction

A severe respiratory coronavirus disease 2019 (COVID-19) caused by SARS-CoV-2 (Severe Acute Respiratory Syndrome Coronavirus 2) has emerged as a pandemic at the end of 2019 (Du et al., 2020; Zhu et al., 2020). By July 2020, SARS-CoV-2 has affected more than 200 territories, infecting more than 13 million individuals and causing more than 0.5 million deaths (WHO, Situation Report–177). COVID-19 has marked the history with third life-threatening coronavirus epidemic into the human population during 21st century (Guo et al., 2020). By 7th January, 2020, Chinese scientists released the sequenced SARS-CoV-2 genome for the identification and development of potential candidates against COVID-19 by computational methods and other therapeutic techniques (Lu et al., 2020).

The SARS-CoV-2 is a β-coronavirus, enveloped and positive sense-RNA virus, with ~30 kb genome (Wu et al., 2020). SARS-CoV-2 genome possesses a complex organization encoding various structural as well as non-structural proteins (Nsps) (Kim et al., 2020a). Majority part of viral genome (replicase ORF1ab encompassing Nsps) is translated into two overlapping polyproteins known as pp1a and pp1ab

* Corresponding author.
E-mail addresses: drazharrasul@gmail.com, azharrasul@gcuf.edu.pk (A. Rasul).

https://doi.org/10.1016/j.phymed.2020.153310
Received 19 April 2020; Received in revised form 19 July 2020; Accepted 19 August 2020
Available online 22 August 2020

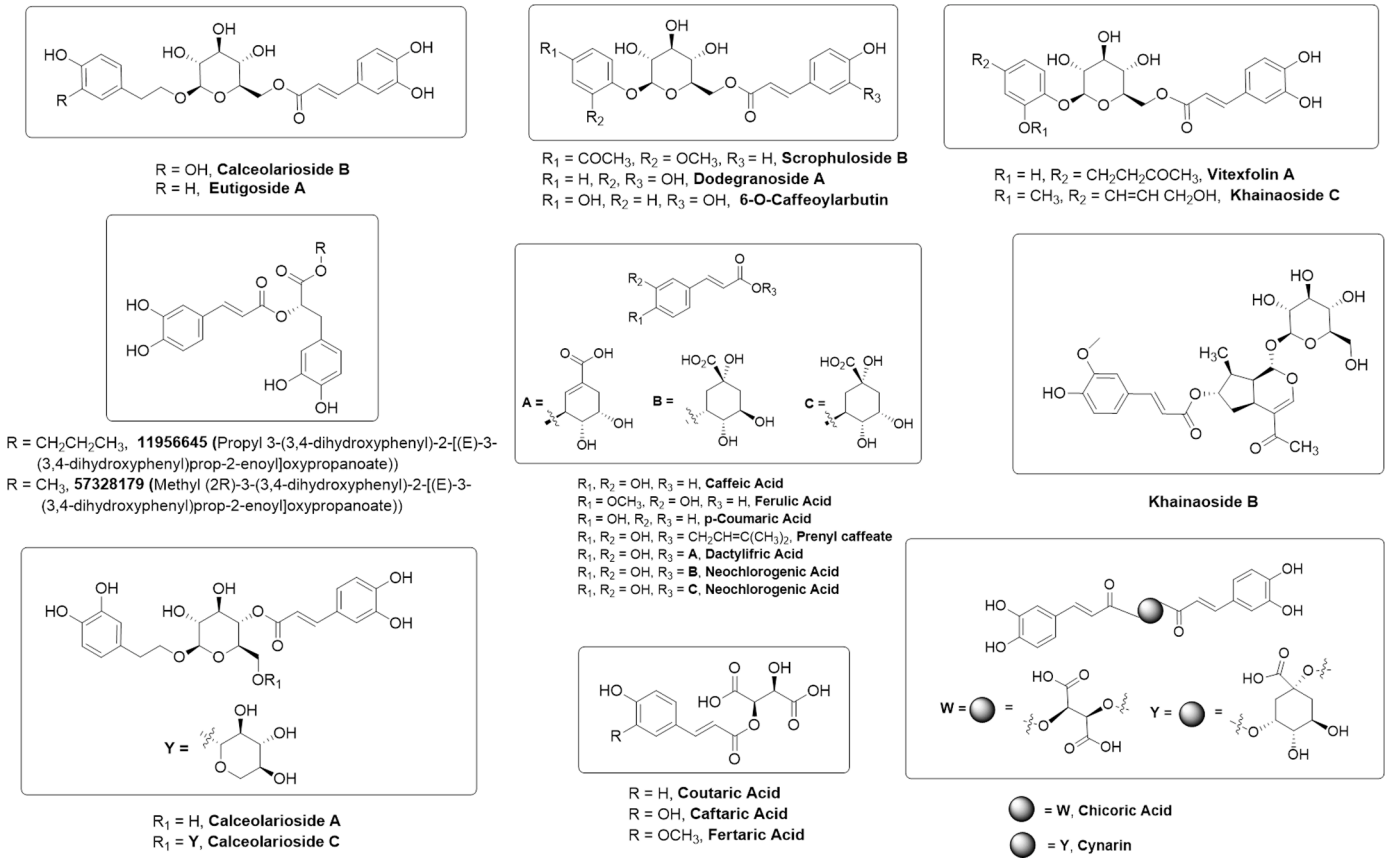

Fig. 1. Chemical structures of caffeic acid and its derivatives.

(Amoretti et al., 2002). These polypeptides also codes for ~306 amino acid long main protease (M^{pro}) (Liu and Wang, 2020), which digests polypeptides at various conserved sites yielding 16 functional viral Nsps possessing multiple enzymatic activities especially in viral replication (Amoretti et al., 2002; Kim et al., 2020a). One of such enigmatic protein, Nsp15, is an endoribonuclease known to be indispensable for protein interference during innate immune response (Kim et al., 2020a). Due to functional importance of M^{pro} and Nsp15 in viral replication and survival, both could be potential therapeutic drug targets to combat COVID-19.

In addition to Nsps, SARS-CoV-2 genome also consists of structural protein encoding genes including S (spike) gene, E gene (viral envelop protein), and N (nucleo-capsid protein) gene (Khan et al., 2020). Viral spike proteins possess strong affinity with the human ACE2 (angiotensin-converting enzyme 2) receptor by which virus fuses with target membrane to gain entry into human cells (Hussain et al., 2020). SARS-CoV-2 fusion potential and ACE2 affinity is much greater as compared to SARS-CoV, suggesting that the SARS-CoV-2 fusion machinery is a novel target for coronavirus fusion inhibitors. S protein binds ACE2 receptor via its S1 subunit, while its S2 subunit interacts to form fusion core, which brings viral and target cell membranes into proximity for efficient fusion and subsequent infection (Xia et al., 2020). Thus, SARS-CoV-2 S2 subunit could be a potential target for coronavirus fusion inhibitors. Moreover, S1 trimeric crowns removal or opening is expected to be essential for exposure of receptor binding domain (RBD) to ACE2 receptor and S2 conformational changes which enable binding and membrane fusion (Walls et al., 2020b) suggesting that SARS-CoV-2 spike ectodomain structure and SARS-CoV-2 spike closed state glycoprotein structure might be novel therapeutic targets to develop anti-COVID-19 drugs.

Growing evidences have established the worth of polyphenols as lead compounds for drug discovery against various human diseases (Dos Santos et al., 2018). Recent studies reported that polyphenol have potential to combat with COVID-19 (Adem et al., 2020). Caffeic acids are one of the abundant plant-based polyphenols possessing 2 phenolic hydroxyl moieties and commonly found in coffee, fruits and vegetables (Magnani et al., 2014). Caffeic acids have been reported for their potent virucidal activity against herpes simplex virus (Langland et al., 2018), SFTS (severe fever with thrombocytopenia syndrome) virus (Ogawa et al., 2018), and influenza virus (Utsunomiya et al., 2014). Based upon these results, we have screened a library of caffeic acid derivatives (CAFDs) (Fig. 1) for the identification of novel natural anti-COVID-19 compounds against various SARS-CoV-2 drug targets including COVID-19 M^{pro} (6LU7), SARS-CoV-2 S2 subunit (6LXT), Nsp15 endoribonuclease (6VWW), SARS-CoV-2 spike ectodomain open state structure (6VYB), and SARS-CoV-2 spike closed state glycoprotein structure (6VXX). Our results present in silico-based identification of khainaoside C, 6-O-Caffeoylarbutin, khainaoside B, khainaoside C and vitexfolin A as potent modulators of COVID-19 M^{pro}, Nsp15, coronavirus fusion protein, spike open state and closed state structure respectively. Our findings will provide valuable data for exploration and development of caffeic acid-derivatives as lead structures, novel therapeutic and prophylaxis agents against COVID-19 in the near future.

Methods

To obtain binding interactions between CAFDs and binding pockets of 5 different proteins of SARS-CoV-2, five independent docking analyses were performed by using Molegro Virtual Docker (MVD) software in a computer cluster system provided by EXPER, model-FQC-01266 running Intel Core i3–2100 CPU @3.10GHz Processor, 64 BİT, 4 GB RAM, 1TB hard disk, and NVIDIA GeForce GT 630 Graphic card. The crystal structures of the following SARS-CoV-2 proteins were retrieved from the protein data bank web site (http://www.rcsb.org/pdb): SARS-CoV-2 M^{pro} (PDB ID: 6LU7: Resolution 2.16 Å) (Jin et al., 2020), Nsp15 endoribonuclease (PDB ID: 6VWW) (Kim et al., 2020b), coronavirus

Table 1
Results of the docking of CAFDs on the crystal structure of COVID-19 virus M^{pro} (6LU7)

Ligand	MolDock Score	Protein-Ligand Interactions	Internal Ligand Interactions	H-Bond
Nelfinavir	-147.3800	-171.698	22.284	-6.8731
Khaınaosıde C	-191.599	-200.025	8.42644	-27.1197
Calceolarioside B	-191.295	-192.449	1.15387	-29.335
Vitexfolin A	-186.282	-195.849	9.56729	-27.845
Calceolarioside C	-178.554	-230.49	51.9361	-26.4726
Scrophuloside B	-177.799	-174.45	-3.34965	-13.1931
Cynarin	-177.1841	-207.737	30.5529	-20.6951
Eutıgosıde A	-167.291	-178.443	11.1524	-19.147
Calceolarioside D	-165.78	-173.156	7.37642	-19.0178
Robustaside D	-164.794	-181.854	17.0598	-31.946
Chicoric acid	-162.6854	-178.756	16.0706	-18.3829
Robustaside E	-161.535	-177.951	16.4157	-24.393
Dodegranoside A	-157.933	-192.633	34.6997	-32.2933
6-O-Caffeoylarbutin	-156.602	-166.442	9.84068	-17.4251
Khaınaosıde B	-155.284	-185.867	30.5834	-21.4445
Calceolarioside A	-149.67	-174.029	24.3592	-24.5915
Propyl 3-(3,4-dihydroxyphenyl)-2-[(E)-3-(3,4-dihydroxyphenyl) prop-2-	-148.144	-166.589	18.4446	-11.8087
Methyl (2R)-3-(3,4-dihydroxyphenyl)-2-[(E)-3-(3,4-dihydroxyphenyl) prop-2-enoyl] oxypropanoate	-145.999	-165.943	19.944	-10.591
Dactylifric acid,	-134.2368	-156.667	22.4302	-19.4056
Neochlorogenic acid	-130.0202	-159.793	29.7728	-21.9994
Fertaric acid	-127.1668	-144.398	17.2312	-12.0719
Prenyl caffeate acid	-122.69655	-130.602	7.90545	-5.00251
Caftaric acid	-121.9308	-145.024	23.0932	-12.1007
Chlorogenic acid	-119.6166	-147.503	27.8864	-14.8102
Coutaric acid	-119.1713	-136.215	17.0437	-10.6761
Caffeic acid	-91.5046	-100.307	8.80237	-12.4985
p-Coumaric acid	-90.0385	-98.9344	8.89594	-6.95915
Ferulic	-78.5495	-83.6803	5.13082	-4.9909

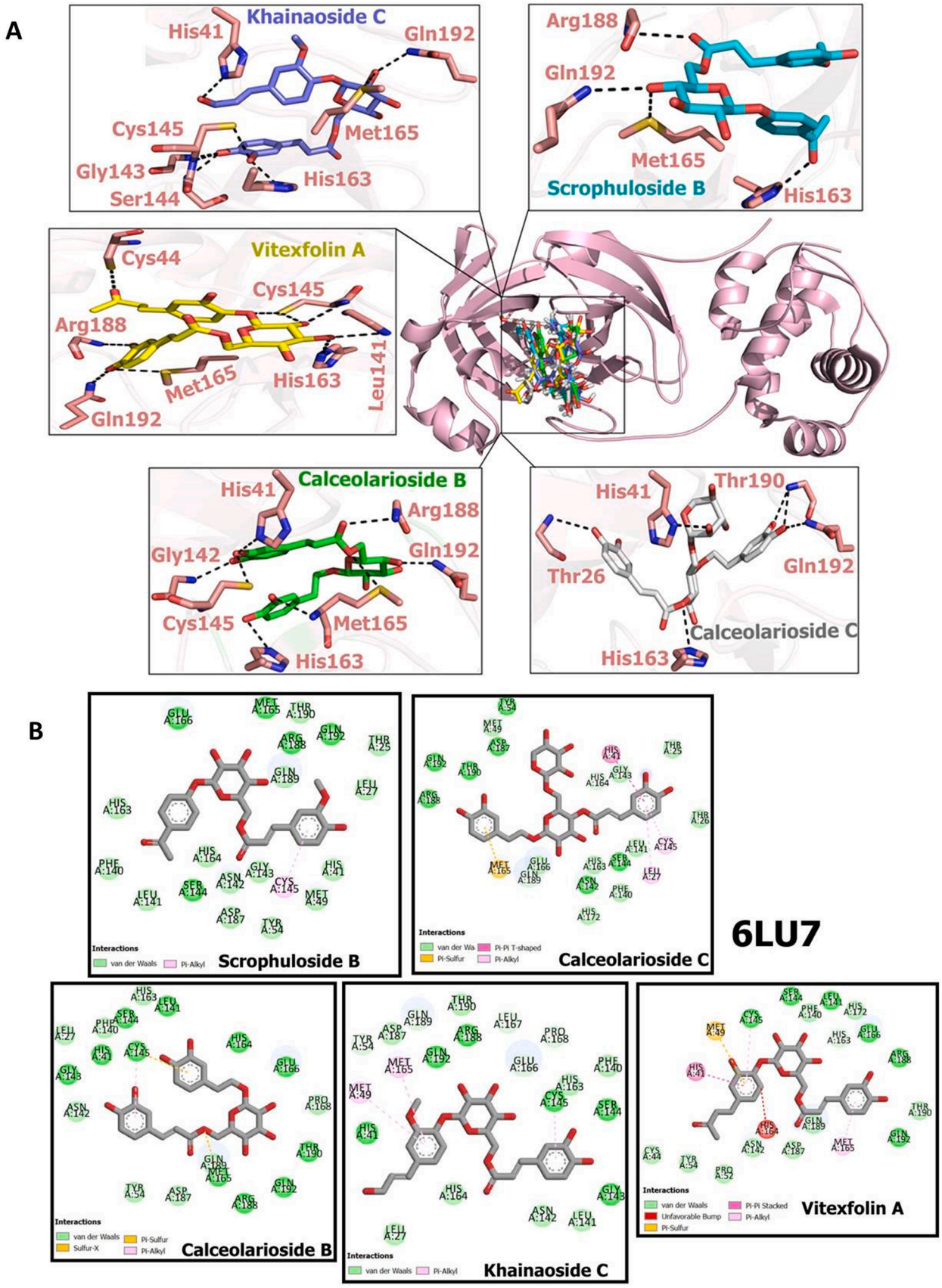

Fig. 2. Docking poses of caffeic acid derivatives with COVID-19 virus M^{pro} **(A)** Hydrogen bonding interactions of khaınaosıde C, scrophuloside B, vitexfolin A, calceolarioside B and calceolarioside C with amino acid residues of COVID-19 virus M^{pro}, **(B)** 2D view of interaction types of khaınaosıde C, scrophuloside B, vitexfolin A, calceolarioside B and calceolarioside C with surrounding amino acids of COVID-19 virus M^{pro}.

Table 2
Results of the docking of CAFDs on the crystal structure of Nsp15 endoribonuclease (6VWW).

Ligand	MolDock Score	Protein-Ligand Interactions	Internal Ligand Interactions	H-Bond
Nelfinavir	-148.413	-176.918	28.5042	-6.24452
6-O-Caffeoylarbutin	-171.541	-192.585	21.0444	-21.747
Dodegranoside A	-168.82	-189.321	20.5011	-20.0539
Calceolarioside B	-164.77	-178.002	13.2327	-16.1947
Scrophuloside B	-163.023	-188.728	25.7045	-17.7
Calceolarioside A	-157.557	-191.866	34.3089	-22.6471
Calceolarioside D	-157.531	-176.714	19.1827	-13.5793
Robustaside D	-152.212	-166.649	14.4366	-13.1528
Vitexfolin A	-151.664	-174.554	22.8901	-14.0706
Eutıgosıde A	-150.42	-173.682	23.2626	-14.3851
Robustaside E	-150.175	-181.359	31.1841	-20.7424
Chicoric acid	-149.662	-165.153	15.4907	-9.06476
Propyl 3-(3,4-dihydroxyphenyl)-2-[(E)-3-(3,4-dihydroxyphenyl) prop-2-	-148.42	-160.41	11.9901	-11.2875
Khaınaosıde B	-146.216	-159.431	13.2149	-18.838
Khaınaosıde C	-144.449	-169.295	24.8469	-14.338
Calceolarioside C	-143.258	-190.29	47.0315	-26.9485
Methyl (2R)-3-(3,4-dihydroxyphenyl)-2-[(E)-3-(3,4-dihydroxyphenyl) prop-2-enoyl] oxypropanoate	-136.959	-151.082	14.1226	-7.66985
Cynarin	-136.239	-168.638	32.3994	-9.84515
Dactylifric acid	-124.395	-135.853	11.4586	-11.8072
Chlorogenic acid	-117.22	-146.224	29.004	-19.2892
Fertaric acid	-115.811	-131.072	15.2609	-10.3567
Neochlorogenic acid (NCHL)	-114.913	-140.215	25.3017	-13.8222
Prenyl caffeate acid	-113.339	-118.376	5.03646	-9.94435
Coutaric acid	-112.946	-123.273	10.3278	-9.20319
Caftaric acid	-110.286	-130.278	19.9917	-13.6044
p-Coumaric acid	-90.4353	-98.5634	8.12807	-7.41811
Caffeic acid	-86.1121	-92.4587	6.34661	-7.61903
Ferulic acid	-78.5357	-83.0275	4.49178	-4.65339

fusion protein (PDB ID: 6LXT) (Xia et al., 2020), SARS-CoV-2 spike ectodomain (PDB ID: 6VYB) and spike glycoprotein (open state) (PDB ID: 6VXX) (Walls et al., 2020a). The selected cavity of 6LU7 is the binding site of natural inhibitor N3. Nelfinavir, utilized for the cure of the HIV (human immunodeficiency virus), was utilized as a positive control. For other targets, the docking cavities of target proteins were selected according to the amino acids involved in the activity of protein. The docking x y z positions of the proteins were identified as-10.87 15 68.21 for 6LU7 (radius 15 Å) −68.51 29.06 29 for 6VWW (radius 14 Å), -20 19 -25 for 6LXT (radius 22 Å), 217 195 265 for 6VXX (radius 24 Å) and 231 185 168 for 6VYB (radius 21 Å). MolDock Score was selected at the scoring function and the search algorithm. After docking, energy minimization and H-bond optimizations were performed. The docking simulation was repeated for each ligand 20 times. The top binding scores were utilized for further analysis. Also, Discovery Studio Visualizer 2020 was used for in-depth analysis of docking results.

The chemical structures of selected compounds were received at 3D SDF conformer from the PubChem site. PubChem CIDs of examined compounds are given respectively; Khainaoside C (44606078), Calceolarioside B (5273567), Vitexfolin A(10458788), Calceolarioside C (45360240), Scrophuloside B (11712581), Cynarin (CYN) (5281769), Eutigoside A (10026568), Calceolarioside D (14015431), Robustaside D (38358972), Chicoric acid (CHA) (5281764), Robustaside E (50994836), Dodegranoside A (44513070), 6-O-Caffeoylarbutin (15689808), Khainaoside B (44606238), Calceolarioside A (5273566), Propyl 3-(3.4-dihydroxyphenyl)-2-[(E)-3-(3.4-dihydroxyphenyl)prop-2-enoyl]oxypropanoate (11956645), Dactylifric acid (6124136), Neochlorogenic acid (NCHL) (5280633), Fertaric acid (FTA) (22298372), Prenyl caffeate acid (5281790), Caftaric acid (CFT) (6440397), Chlorogenic acid (CHL) (1794427), Coutaric acid (CTA) (57517924), Caffeic acid (689043), p-Coumaric acid (637542), Ferulic acid (445858). 3D SDF structures were prepared with ChemBio3D or MarvinSketch for simple molecules.

ADME and toxicity prediction

In silico ADME analysis was conducted to investigate physicochemical properties of potent hits, such as water solubility, lipophilicity and pharmacokinetics by using following website http://www.swissadme.ch (Daina et al., 2017). Absorption (% ABS) of potent hits from intestine was evaluated by: % ABS = 109 × (0.345xTPSA). Toxicity analysis was performed using offline software Toxtree 3.1 application (Zhao et al., 2002).

Molecular dynamics study

The structures of the best-docked complex for each protein are selected for in-depth molecular dynamics simulation (MDS) study for a period of 20 ns. NAMD software was utilized to conduct the MDS with CHARMM 36 force field (Huang and MacKerell, 2013; Phillips et al., 2005). VMD is used to prepare the complexes for the MDS (Humphrey et al., 1996). Complexes are subjected to equilibration using the CHARMM GUI web server after that a production run for 20 ns is performed on Shaheen supercomputer of King Abdullah University of Science and Technology (KAUST) under the project number k1482 (Jo et al., 2008). The equilibration is done on the protein-small molecule solvated in the TIP3P water model and 0.154 M NaCl solution at 310 K temperature and pH 7 (Mark and Nilsson, 2001). VMD is utilized in trajectories analysis, while the Chimera software of UCSF is used for cluster analysis (Mark and Nilsson, 2001; Pettersen et al., 2004). After trajectory clustering, the five most populous clusters are represented by a conformation and tested for its binding to the protein. AutoDock Vina software is used in the binding energy calculations using 40 Å × 40 Å × 40 Å box dimensions (Morris et al., 2009; Trott and Olson, 2010).

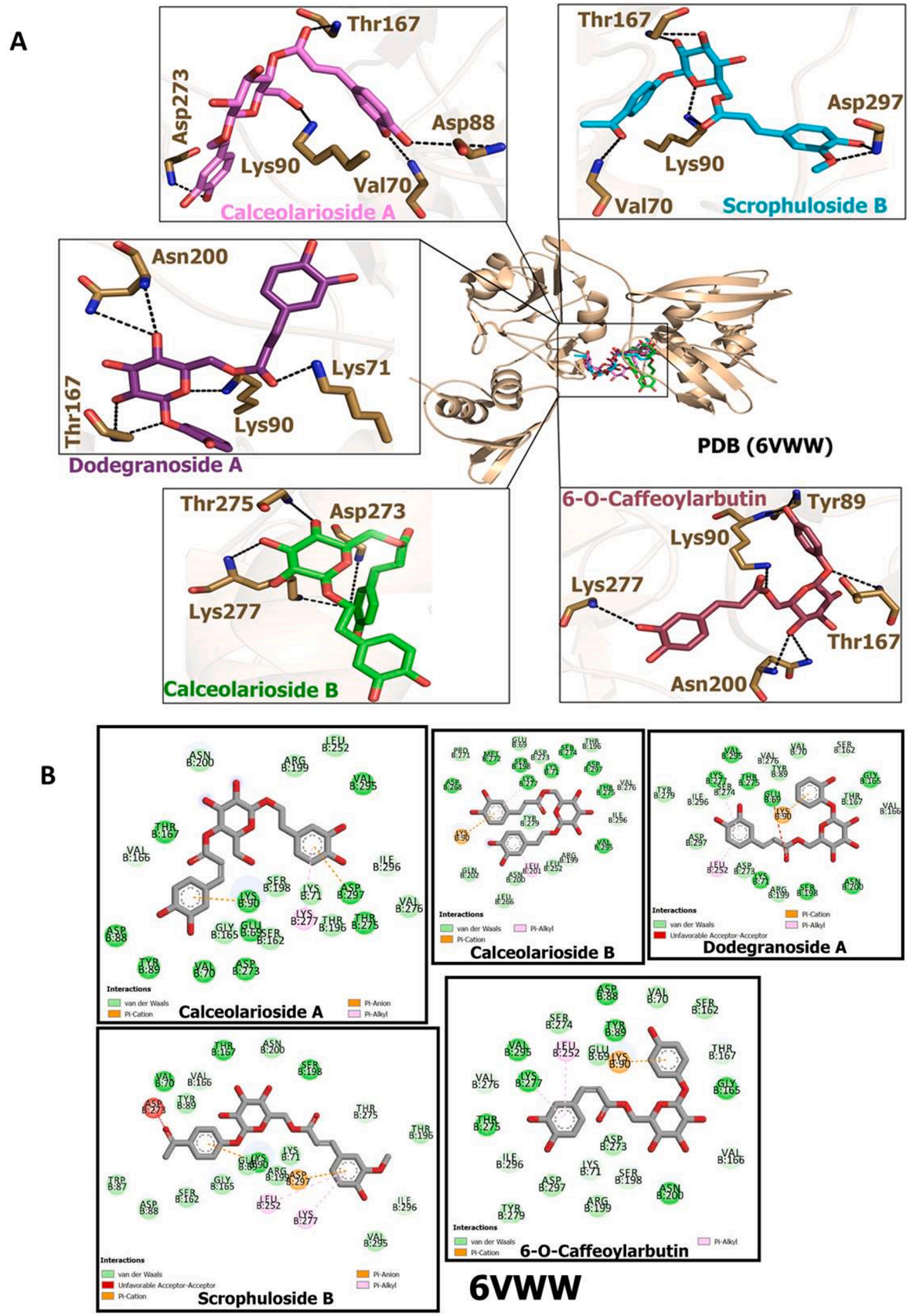

Fig. 3. Docking poses of caffeic acid derivatives with COVID-19 virus Nsp15 endoribonuclease **(A)** Hydrogen bonding interactions of 6-O-Caffeoylarbutin, calceolarioside B, dodegranoside A, calceolarioside A and scrophuloside B with amino acid residues of virus Nsp15 endoribonuclease **(B)** 2D view of interaction types of 6-O-Caffeoylarbutin, calceolarioside B, dodegranoside A, calceolarioside A and scrophuloside B with surrounding amino acids of COVID-19 virus Nsp15 endoribonuclease.

Table 3
Results of the docking of CAFDs on the crystal structure of post fusion core of SARS-CoV-2 S2 subunit (6LXT).

Ligand	MolDock Score	Protein-Ligand Interactions	Internal Ligand Interactions	H-Bond
Nelfinavir	-130.687	-164.232	33.5452	-9.3432
Khaınaosıde B	-150.44	-161.896	11.4557	-8.36351
Chicoric acid	-150.017	-168.62	18.603	-11.1833
Vitexfolin A	-149.558	-185.217	35.6583	-20.1769
6-O-Caffeoylarbutin	-146.12	-164.641	18.5207	-16.9512
Calceolarioside B	-141.587	-172.326	30.7394	-11.9822
Khaınaosıde C	-139.261	-147.331	8.06987	-11.3859
Calceolarioside D	-138.843	-151.697	12.8542	-8.86834
Calceolarioside A	-135.155	-170.652	35.4964	-13.9423
Scrophuloside B	-134.911	-150.3	15.3891	-11.735
Robustaside D	-132.712	-148.2	15.488	-8.16426
Calceolarioside C	-132.021	-171.948	39.9268	-21.5846
Cynarin	-129.89	-173.962	44.0712	-15.3668
Eutıgosıde A	-129.684	-148.713	19.0289	-10.3091
Dodegranoside A	-129.625	-153.199	23.5741	-8.37051
Robustaside E	-128.164	-158.032	29.8676	-14.1894
Propyl 3-(3,4-dihydroxyphenyl)-2-[(E)-3-(3,4-dihydroxyphenyl) prop-2-	-125.955	-141.065	15.1099	-5
Methyl (2R)-3-(3,4-dihydroxyphenyl)-2-[(E)-3-(3,4-dihydroxyphenyl) prop-2-enoyl] oxypropanoate	-120.097	-139.184	19.087	-10.5192
Neochlorogenic acid	-112.361	-138.544	26.183	-15.9721
Fertaric acid	-106.658	-131.958	25.3	-9.22242
Dactylifric acid	-106.238	-127.635	21.3977	-12.3803
Caftaric acid	-104.253	-120.779	16.5262	-10.7807
Coutaric acid	-103.181	-114.849	11.6674	-9.25386
Chlorogenic acid	-101.663	-127.123	25.4594	-12.0677
Prenyl caffeate acid	-96.4395	-106.955	10.5154	-7.95977
p-Coumaric acid	-77.652	-84.3751	6.72302	-8.07627
Caffeic acid	-70.7393	-77.8201	7.08078	-8.17656
Ferulic	-68.4726	-74.5274	6.05481	-5.1854

Results

The MolDock Scores obtained from the docking studies of CAFDs and 6LU7 are summarized in Table 1. Based on these in-silico results, khainaoside C, calceolarioside B, vitexfolin A, calceolarioside C and scrophuloside B exhibited best binding potential with COVID-19 virus M^{pro} having MolDock scores of -191.5990, -191.2950, -186.2820, -178.5540 and -177.799 respectively. Khainaoside C showed the highest binding affinity at the active site. It forms hydrogen bond interactions with His 41, His 163, Met 165, Arg 188, Gln 192, Glu 166, Cys 145, Gly 143, Ser 144, Leu 141 (Fig. 2A). Calceolarioside B binds to SARS-CoV-2 M^{pro} by forming hydrogen bonds with His 41, His 163, His 164, Met 165, Asp 187, Gln 189, Thr 190, Arg 188, Gln 192, Glu 166, Cys 145, Gly 143, Ser 144, Leu 141 (Fig. 2A). Vitexfolin A and calceolarioside C also showed good binding affinities to the active sites of COVID-19 virus M^{pro} via interacting with Met 49, Tyr 54, Cys 44, His 163, His 164, Arg 188, Gln 192, Glu 166, Cys 145, Ser 144, Leu 141, Phe 140 (Fig. 2A) and His 41, Tyr 54, Thr 26, His 163, His 164, Met 165, Asp 187, Gln 189, Thr 190, Arg 188, Gln 192, Glu 166, Asn 142, Cys 145, Ser 144, Leu 141 respectively (Fig. 2A). According to the obtained results, khainaoside C and calceolarioside B affinities with COVID-19 virus M^{pro} and their scores are significantly higher than Nelfinavir. Ligand plot in Fig. 2B represents residual wise van der Waals interactions, pi-alkyl interactions, pi-pi interactions and pi-sulfur interactions of potent hits with M^{pro}.

The MolDock Scores obtained from the docking studies of CAFDs and 6VWW are provided in Table 2. 6-O-Caffeoylarbutin, dodegranoside A, calceolarioside B, scrophuloside B and calceolarioside A possess significantly good binding potential to Nsp15 endoribonuclease with MolDock Scores -171.541, -168.82, -164.77, -163.023 and -157.557 respectively as compared to Nelfinavir which possess MolDock score of -148.413 The interactions of these compounds with amino acid residues of target protein are shown in Fig. 3A. Ligand plot representing residual wise van der Waals interaction, pi-alkyl interactions, pi-cation and pi-anion interactions are presented in Fig. 3B.

Table 3 presents MolDock Score, interactions and H-Bonds obtained from the docking studies of CAFDs with 6LXT. The results show highest binding potential of khaınaosıde B (-150.44), followed by chicoric acid (-150.017), vitexfolin A (-149.558) 6-O-Caffeoylarbutin (-146.12) and calceolarioside B (-141.587) as compared to Nelfinavir (-130.687). The binding interactions of potent compounds with S2 subunit of fusion protein are shown in Fig. 4A. Fig. 4B shows residual wise van der Waals interactions, pi-alkyl interactions, pi-pi interactions, amide-pi-stacked interactions and pi-anion interactions of potent hits with 6LXT.

Table 4 shows the obtained results from the docking studies of CAFDs with crystal structure 6VYB. The results show highest binding potential of khaınaosıde C (-166.448), followed by khaınaosıde B (-165.435), and calceolarioside B (-153.135), calceolarioside C (-151.284), and calceolarioside D (-149.841) with comparison to reference drug Nelfinavir (-148.747). The amino acid residues of spike protein participating in interaction with these compounds are presented in Fig. 5A. CAFDs interact with target protein via van der Waals interactions, pi-alkyl interactions, pi-pi interactions, amide-pi-stacked interactions and pi-sigma interactions (Fig. 5B).

The binding energies obtained from the docking analysis of 6VXX with ligands are presented in Table 5. Vitexfolin A, chicoric acid, eutıgosıde A exhibited the best potential against spike glycoproteins of SARS-CoV-2. According to in silico results, 7 of the compounds have a better affinity to bind with spike glycoproteins than Nelfinavir (Table 5). The ligand-protein interactions are shown in Fig. 6A. Amino acid residues of 6VXX interact with CAFDs via van der Waals interaction, pi-alkyl interactions, pi-pi interactions and pi-sigma interactions are (Fig. 6B).

Among all the screened compounds, only calceolarioside B possess good binding affinities with four out of five selected targets of SARS-CoV-2 (COVID-19 virus M^{pro}, Fusion S2 subunit, spike ectodomain (open state), and Nsp15 endoribonuclease) while vitexfolin A exhibits

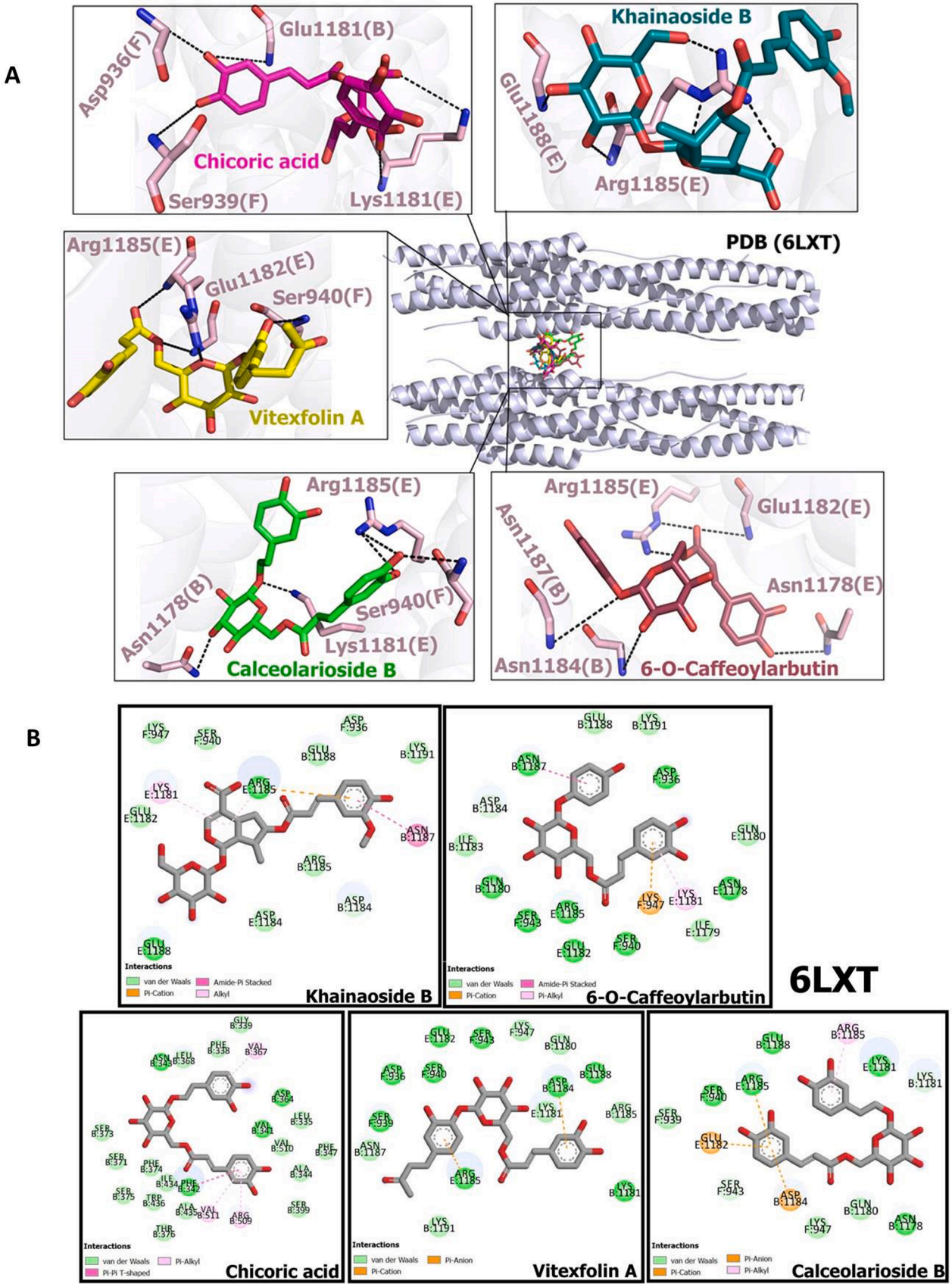

Fig. 4. Docking poses of caffeic acid derivatives with COVID-19 virus fusion protein S2 subunit **(A)** Hydrogen bonding interactions of khaınaosıde B, chicoric acid, vitexfolin A, 6-O-Caffeoylarbutin, and calceolarioside B with amino acid residues of fusion protein S2 subunit **(B)** 2D view of interaction types of khaınaosıde B, chicoric acid, vitexfolin A, 6-O-Caffeoylarbutin, and calceolarioside B with surrounding amino acids of COVID-19 virus fusion protein S2 subunit.

Table 4
Results of the docking of CAFDs on the crystal structure of SARS-CoV-2 spike ectodomain structure (open state) (6VYB).

Ligand Name	MolDock Score	Protein-Ligand Interactions	Internal Ligand Interactions	H-Bond
Nelfinavir	-148.747	-176.89	28.1432	-2.49896
Khaınaosıde C	-166.448	-161.803	-4.64496	-8.71808
Khaınaosıde B	-165.435	-193.843	28.408	-9.1829
Calceolarioside B	-153.135	-177.198	24.0631	-11.6422
Calceolarioside C	-151.284	-203.133	51.8485	-15.5073
Calceolarioside D	-149.841	-171.435	21.5938	-6.20592
Eutıgosıde A	-144.298	-150.757	6.45875	-8.94751
Dodegranoside A	-142.831	-161.943	19.1118	-6.51745
Vitexfolin A	-142.604	-173.882	31.278	-12.4266
Chicoric acid	-141.566	-164.796	23.2302	-6.62961
Propyl 3-(3,4-dihydroxyphenyl)-2-[(E)-3-(3,4-dihydroxyphenyl) prop-2-	-139.154	-149.85	10.6965	-6.13396
6-O-Caffeoylarbutin	-137.225	-160.96	23.7351	-9.99943
Cynarin	-133.964	-180.052	46.0882	-3.61595
Robustaside D	-133.688	-139.895	6.20761	-7.9848
Calceolarioside A	-133.035	-170.659	37.6243	-13.4663
Robustaside E	-132.278	-154.031	21.7532	-4.63369
Methyl (2R)-3-(3,4-dihydroxyphenyl)-2-[(E)-3-(3,4-dihydroxyphenyl) prop-2-enoyl] oxypropanoate	-129.816	-140.552	10.7361	-3.44702
Scrophuloside B	-129.274	-159.233	29.959	-5.75544
Neochlorogenic acid	-116.183	-137.163	20.9802	-8.85752
Dactylifric acid	-114.666	-128.192	13.5263	-5.90671
Fertaric acid	-111.217	-123.587	12.3705	-2.53938
Caftaric acid	-109.539	-124.99	15.4504	-9.02851
Prenyl caffeate acid	-109.296	-118.722	9.42623	-3.47987
Chlorogenic acid	-108.993	-132.887	23.8942	-8.6096
Coutaric acid	-103.861	-113.724	9.86261	-2.97925
p-Coumaric acid	-87.9961	-96.8163	8.82013	-4.60597
Caffeic acid	-85.3883	-91.7692	6.38084	-7.06512
Ferulic	-83.9251	-89.969	6.04391	-2.71179

good binding efficacy against three out of five selected proteins of SARS-CoV-2 (COVID-19 virus M^{pro}, Fusion S2 subunit and spike protein). Based upon these findings, calceolarioside B could be regarded as pan inhibitor of SARS-CoV-2 proteins.

Relative assessment of MolDock scores were performed with (β), of CAFDs against SARS-CoV-2 proteins encoded by PDB IDs as **6LU7, 6VWW, 6TLX, *6VYB,*** and ***6VXX*** (Fig. 7). We normalized all MolDock scores using equation as described below

$$\beta_N = \beta_i / \beta_{max}$$

Where; β_N, β_i, β_{max} represent the normalized MolDock score, MolDock score of a compound for any drug target protein and maximum MolDock score among all compounds of any drug target protein.

ADME profiling of potent caffeic acid derivatives

The eight compounds with high-binding affinity against COVID-19 were analysed for ADME properties using SwissADME web tool. The results of eight compounds with high activity potential are presented in Fig. 8. Eutigoside A meets all criteria for oral use. Physicochemical, pharmacokinetics and drug-likeness properties of potent hits are presented in Table 6. All of the compounds are water soluble. They do not cross the blood brain barrier, do not interact with interaction of main enzymes of Cytochromes P450, and have P-gp substrate properties. Toxicity assessment according to the chemical structure was carried out using Toxtree software.

Molecular dynamics simulation

Fig. 9A shows the Root Mean Square Deviation (RMSD) in Å, Radius of Gyration (RoG) in Å, and Surface Accessible Surface Area (SASA) in Å2. The values of the three parameters indicate the equilibration of the systems during the 20 ns MDS. On the other hand, Fig. 9B shows the stability of the residues during the simulation through per residue Root Mean Square Fluctuation (RMSF) in Å. Dashed-red lines indicate the positions of the active site residues. Fig. 9C shows the average binding energies obtained for the representative conformation for each cluster after the MDS run for 20 ns on the protein-ligand complexes.

Discussion

Polyphenols possess various beneficial properties against viral diseases such as modulation of immune system (Jasso-Miranda et al., 2019), inhibiting viral replication (Lalani and Poh, 2020) and reduction of viral uptake by target membrane (Vazquez-Calvo et al., 2017). CAFDs are polyphenolic compounds which possess prominent antiviral activity especially against hepatitis B virus (HBV) (Zhang et al., 2014) and HIV (Pluymers et al., 2000). Keeping in view the potential of CAFDs against viral diseases (Fig. 1), 27 CAFDs were docked with 5 proteins of SARS-CoV-2 to evaluate their binding energies against these targets. Out of 27 CAFDs, 19 of them showed greater MD score (ranging between -191 to -159, Table 1) against COVID-19 virus M^{pro} as compared to nelfinavir (-147) (Adem et al., 2020). 11 out of 27 CAFDs possess greater MD score against Nsp15 endoribonuclease (Table 2) and SARS-CoV-2 fusion S2 subunit as compared to reference drug (Table 3), while 5 were found to be good binder of spike ectodomain (open state) (Table 4) and 7 exhibits good binding interaction with spike glycoprotein (closed state) as compared to Nelfinavir (Table 5). From chemical point of view, the binding potential of potent CAFDs i.e., khainaoside C, scrophuloside B, vitexfolin A, calceolarioside B & C with SARS-CoV-2 proteins can largely be attributed to the presence of hydroxyl and carbonyl groups. These groups specifically –OH group serves as excellent candidate for hydrogen bonding and exhibits tendency to form strong interactions with amino acid residues of target protein. As reported in Fig. 9, the 20 ns MDS runs were enough for the protein-ligand complexes. RMSD for

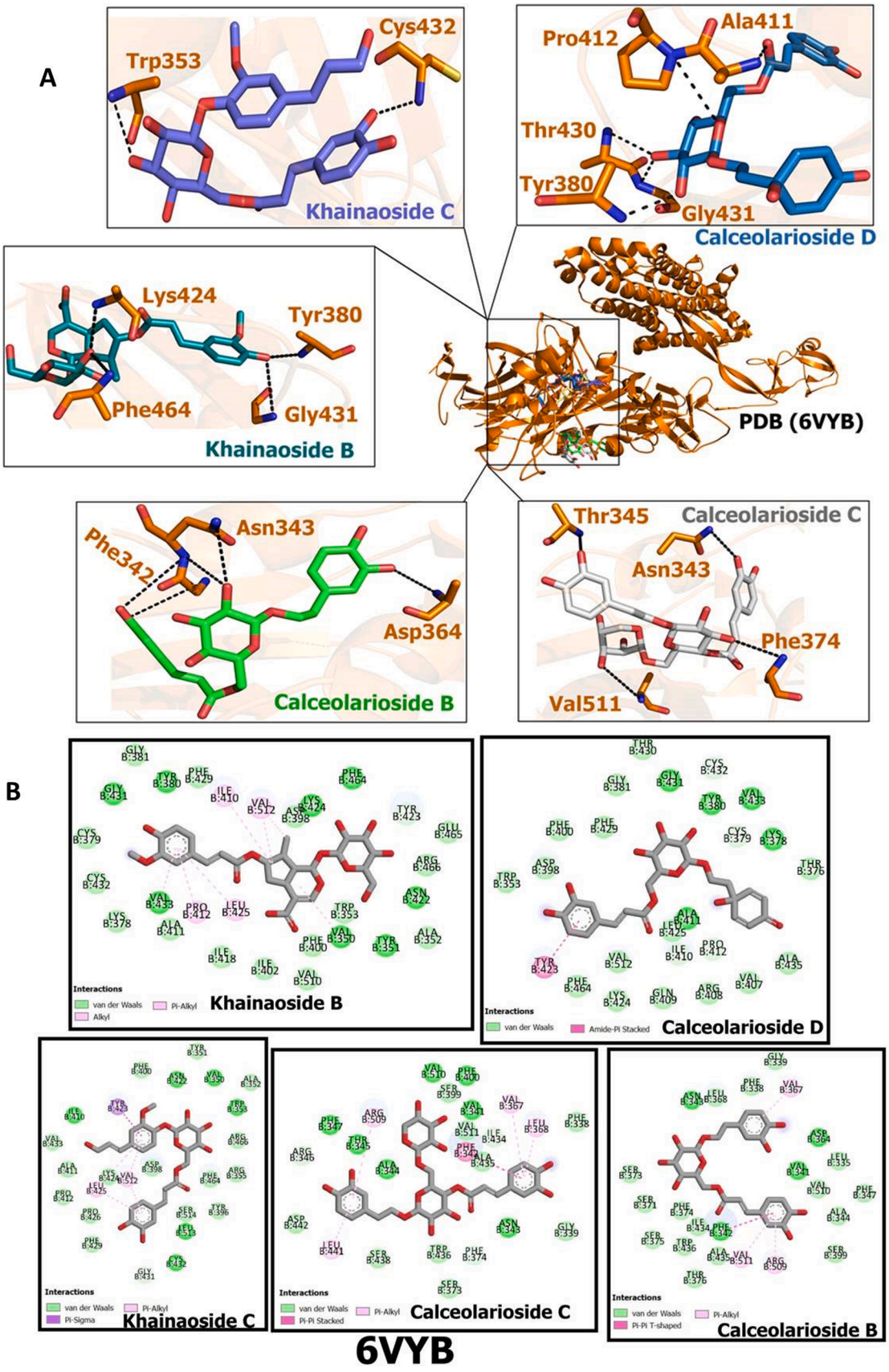

Fig. 5. Docking poses of caffeic acid derivatives with SARS-CoV-2 spike ectodomain **(A)** Hydrogen bonding interactions of khaınaosıde C, khaınaosıde B, calceolarioside B, calceolarioside C, calceolarioside D with amino acid residues of SARS-CoV-2 spike ectodomain (open state) **(B)** 2D view of interaction types of khaınaosıde C, khaınaosıde B, calceolarioside B, calceolarioside C, calceolarioside D with surrounding amino acids of SARS-CoV-2 spike ectodomain (open state).

Table 5
Results of the docking of CAFDs on the crystal structure of SARS-CoV-2 spike glycoprotein (closed state) (6VXX).

Ligand Name	MolDock score	Protein-ligand interactions	Internal ligand interactions	H-Bond
Nelfinavir	-133.655	-160.117	26.4619	-7.62916
Vitexfolin A	-158.443	-177.854	19.4111	-15.769
Chicoric acid	-141.781	-166.842	25.0606	-7.55396
Eutigosıde A	-137.834	-167.189	29.3553	-11.5249
Scrophuloside B	-136.54	-169.158	32.6181	-10.2562
Cynarin	-136.457	-176.339	39.8825	-11.3919
Calceolarioside D	-135.748	-145.865	10.1171	-7.33425
Khaınaosıde B	-134.98	-141.167	6.18667	-14.3158
Robustaside D	-130.586	-154.38	23.7941	-12.9145
Robustaside E	-126.92	-126.404	-0.5159	-14.472
Khaınaosıde C	-126.895	-124.812	-2.0832	-10.5752
Propyl 3-(3,4-dihydroxyphenyl)-2-[(E)-3-(3,4-dihydroxyphenyl) prop-2-	-125.712	-153.822	28.1099	-11.792
Calceolarioside A	-123.256	-152.379	29.1231	-13.9537
Calceolarioside B	-122.232	-149.1	26.8684	-13.6966
6-O-Caffeoylarbutin	-121.921	-116.367	-5.5538	-8.70194
Dodegranoside A	-119.728	-144.496	24.7679	-9.47601
Methyl (2R)-3-(3,4-dihydroxyphenyl)-2-[(E)-3-(3,4-dihydroxyphenyl) prop-2-enoyl] oxypropanoate	-118.965	-140.467	21.502	-14.4652
Calceolarioside C	-116.478	-176.585	60.1073	-21.2389
Dactylifric acid,	-111.795	-132.804	21.0096	-3.32111
Caftaric acid	-106.167	-121.402	15.2351	-12.1219
Coutaric acid	-105.763	-118.798	13.0344	-11.9847
Fertaric acid	-104.402	-115.523	11.1211	-9.61248
Neochlorogenic acid	-102.203	-130.877	28.6741	-9.99063
Prenyl caffeate acid	-100.523	-107.187	6.66386	-2.5
Chlorogenic acid	-92.1219	-117.747	25.6247	-17.3432
Ferulic	-78.2151	-82.4019	4.18678	-0.5326
Caffeic acid	-75.6669	-83.0829	7.41603	-0.37606
p-Coumaric acid	-73.8693	-82.9404	9.07116	-6.05487

each system show equilibration, while SASA and RoG both show stabilities during the MDS. The per-residues RMSF profiles in Fig. 9B indicate the stability of the binding since the interacting residues (H41, C149 in Mpro, K90, T167 in NSP15, R185 in the post-fusion core, N343, Y380, G431 in spike ectodomain, and F342, T430, N437 in spike closed state) have low RMSF values in all the complexes. Additionally, the average binding energies (Fig. 9C) calculated for the different clusters during the MDS runs show that the binding is stable. Hence, the MDS study supports previous docking scores values.

Most of the CAFDs possessing good binding energies with various proteins of SARS-CoV-2 have been isolated from traditionally used medicinal plants such as: khainaoside B and khainaoside C are isolated from Thai medicinal plant *Vitex glabrata* which is traditionally used to support lactation (Luecha et al., 2009) and possess anti-diabetic potential (Somtimuang et al., 2018). Vitexfolin A is an important constituent of *Vitex rotundifolia* and possesses strong analgesic effect (Okuyama et al., 1998). Scrophuloside B has been identified in traditional Chinese medicinal plants including *Picrorhiza scrophulariiflora* (Wang et al., 2013) and *Radix scrophulariae* (Jing et al., 2011). Calceolarioside B has been isolated from *Fraxinus sieboldiana* and *Forsythia suspensea* plants both of which possess anti-inflammatory and anti-viral properties (Kim et al., 2002; Wang et al., 2009). While some of potent CAFDs are found in vegetables and fruits such as: Lettuce (*Lactuca sativa*), a widely consumed leafy vegetable, is found to be enriched with various CAFDs such as chicoric acid and chlorogenic acid (Abu-Reidah et al., 2013). Chicoric acid has been long known as potent anti-viral agent against HIV (Lin et al., 1999) and its mechanism of action involves deactivation of HIV-1 integrase, increased T-lymphoblastoid viability, and down-regulation of reverse transcriptase of HIV-1 (Peng et al., 2019). 6′-O-caffeoylarbutin is abundantly found in *Vaccinium dunalianumas. V. dunalianumas* is a commonly cultivated blueberry species in China and its dried leaf buds as herbal tea while its leaves are used as folk medicine (Li et al., 2016; Luo et al., 2015). Sunflower (*Helianthus annuus*) sprouts (nutritious sunflower lettuce) found to be enriched with cynarin (Sun et al., 2012), recommending these foods as beneficial food choice for COVID-19 patients.

Among all these potent compounds, calceolarioside B is identified as pan-inhibitor of SARS-CoV-2 having potential to target SARS-CoV-2 M^{pro}, Nsp15, coronavirus fusion protein, as well as spike ectodomain which brought excitement about calceolarioside B's potential against COVID-19. Interestingly, calceolarioside B is also an important constituent of *Akebia trifoliata* fruit which is popularized in Asia due to its nutritional values as well as delicious taste and also used as dietary supplement for its various health benefits including anti-microbial and anti-inflammation (Wang et al., 2019), suggesting that *Akebia trifoliata* fruit could potentially help COVID-19 patients to fight this disease. Calceolarioside B has potential to inhibit gp4l transmembrane glycoproteins of HIV (human immunodeficiency virus) (Kim et al., 2002). These glycoproteins play critical role in virus cell fusion with target membrane to enable viral entry into the host cell (Buzon et al., 2010). As calceolarioside B is identified as potent binder of SARS-CoV-2 spike glycoprotein during our study, the results from both of these studies propose calceolarioside B as viral and target membrane fusion inhibitor further strengthening its role against COVID-19.

In addition, calceolarioside B exhibits good anti-RSV (respiratory syncytial virus) effects (Dong et al., 2017) which recommend that calceolarioside B rich foods could be a potential alternative approach for the prevention and treatment of COVID-19. In addition to its anti-viral properties, it has potential to inhibit IL-6 production to exert it anti-inflammatory properties (Jin et al., 2014). COVID-19 patients suffer with severe inflammatory response in the later stages of infection, thus, dual anti-viral/anti-inflammatory properties of this compound makes it ideal candidate for drug development for prevention and treatment of COVID-19. As coronaviruses mutations make it difficult to develop vaccine, so does the single-target drugs. Single-target drugs might encounter low efficacy as the virus mutates. Thus, complex diseases like

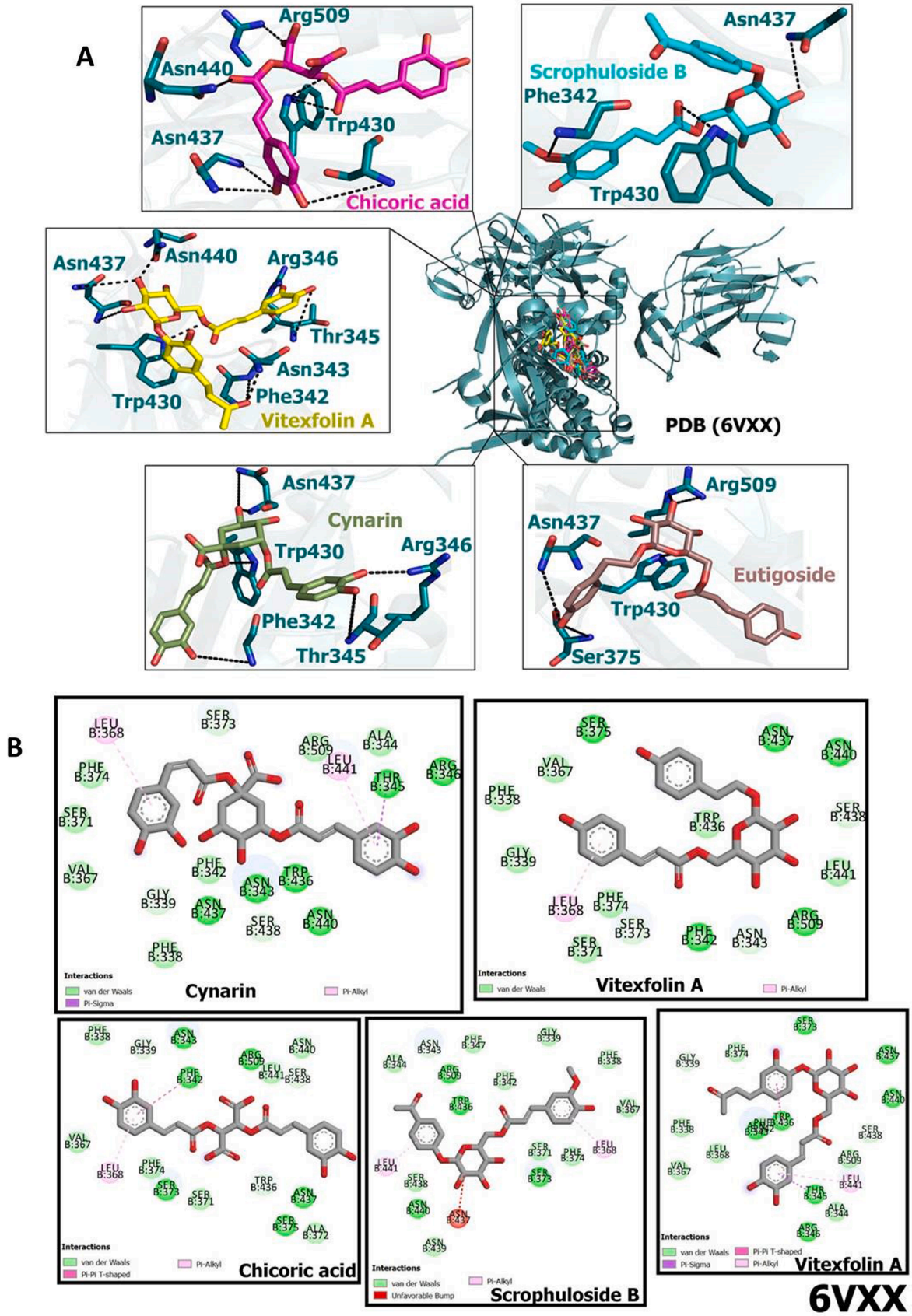

Fig. 6. Docking poses of caffeic acid derivatives with SARS-CoV-2 spike glycoprotein (closed state) **(A)** Hydrogen bonding interactions of scrophuloside B, chicoric acid, vitexfolin A, cynarin and eutıgosıde A with amino acid residues of SARS-CoV-2 spike glycoprotein (closed state) **(B)** 2D view of interaction types of scrophuloside B, chicoric acid, vitexfolin A, cynarin and eutıgosıde A with surrounding amino acids of spike glycoprotein (closed state).

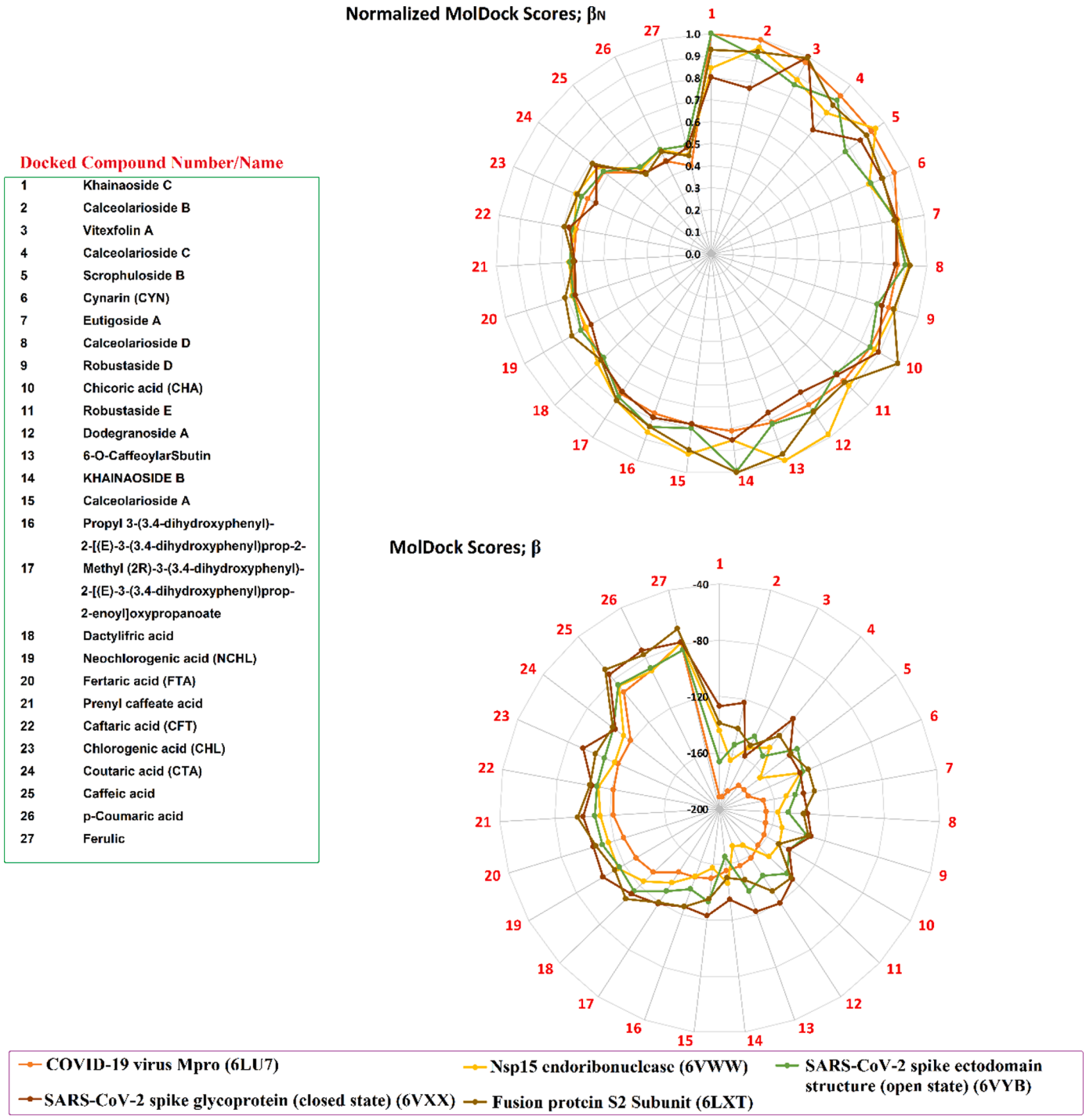

Fig. 7. MolDock Score comparison among 27 compounds versus active sites SARS-CoV-2 6LU7, 6VWW, 6LXT, 6VYB, and 6VXX.

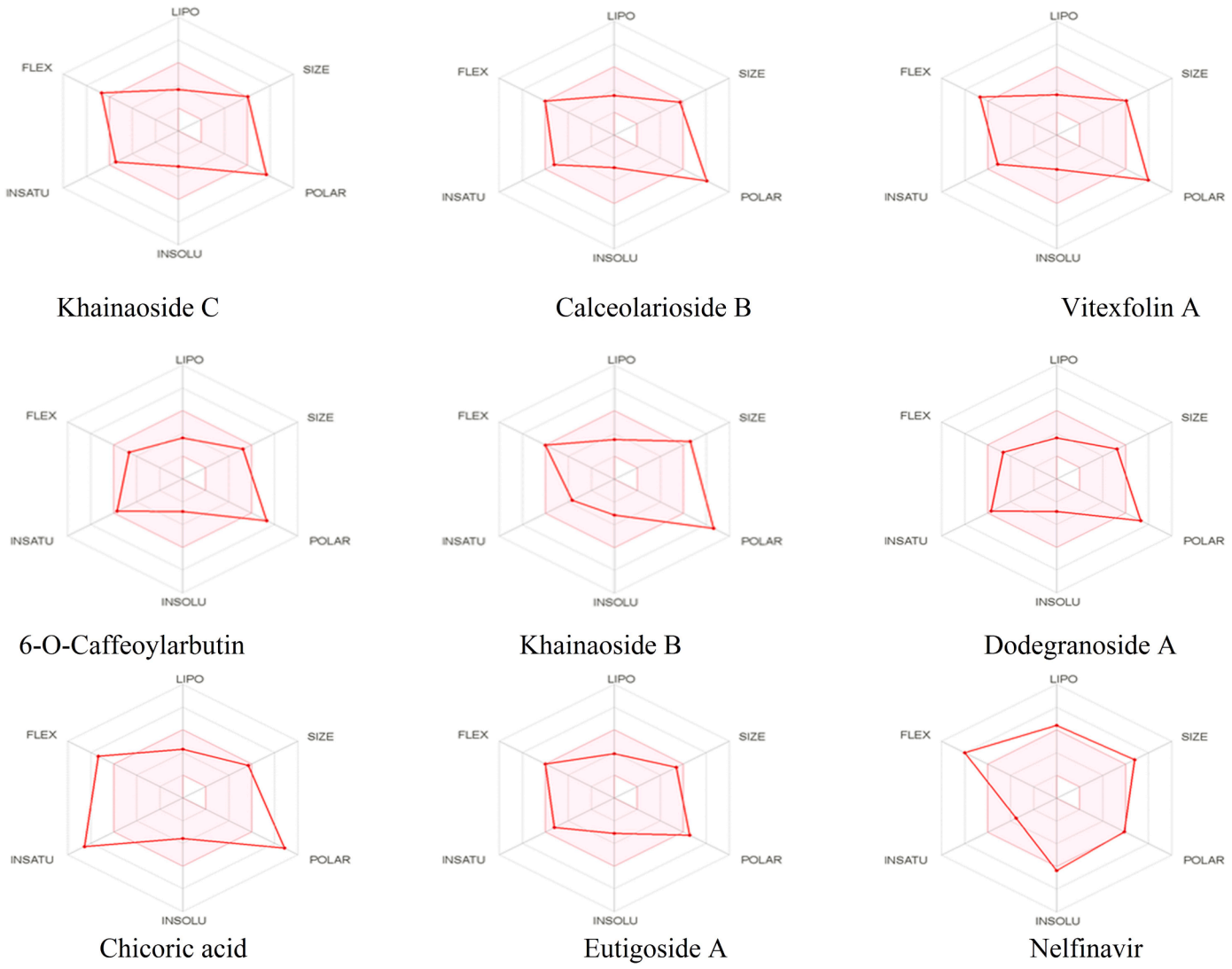

Fig. 8. Bioavailability Radar related to physicochemical properties of molecules (Criterias: Lipophilicity: - 0.7 < XLOGP3 < ++5.0, Size: 150 MW 500 g/mol, Polarity: 20 < TPSA < 130 Å2, Insolubility: 0 < log S < 6, Insaturation, Flexibility: 0.25 < rotatable bonds < 9).

Table 6
ADME profiling of potent caffeic acid derivatives.

Compound name	Ghose	TPSA	Absorption (% ABS)	Water solubilityLog *S* (ESOL)	BBB permeant	P-gp substrate	CYP isoform interact
Khaınaosıde C	No	175.37	48.49	-3.12- Soluble	No	Yes	No
Calceolarioside B	Yes	186.37	44.70	-2.85- Soluble	No	Yes	No
Vitexfolin A	No	183.21	45.79	-3.01- Soluble	No	Yes	No
6-O-Caffeoylarbutin	Yes	166.14	51.68	-2.86- Soluble	No	Yes	No
Khaınaosıde B	No	201.67	39.42	-3.14- Soluble	No	Yes	No
Dodegranoside A	Yes	166.14	51.68	-2.86- Soluble	No	Yes	No
Chicoric acid	Yes	208.12	37.19	-3.58- Soluble	No	Yes	No
Eutıgosıde A	Yes	145.91	58.66	-3.11- Soluble	No	Yes	No
Nelfinavir	No	127.20	65.18	-6.36-Poorly soluble	No	Yes	1A2, 2C19, 3A4

COVID-19 are more likely to be alleviated or healed though simultaneous modulation of multiple targets. Based on the above discussion, in our personal opinion, efficacy of CAFDs-enriched foods against COVID-19 as well as safety suggests that their adoption in daily diets might help prevent the onset of COVID-19 in an alternative and non-pharmacological approach.

Conclusively, this study provides scientific basis for the possible utilization of CAFDs as drug leads to develop anti-COVID-19 therapeutics. Since there is an urgent and timely need to find out effective and specific anti-viral treatment for COVID-19, this study will hopefully lay the foundation to work forward on small scale studies for the determination of 1) efficacy of CAFDs in reducing viral load and shortening the infectious period, 2) optimal dosing regimen based on impact on viremia, 3) impact on antibody production, inflammatory signaling and oxidative stress in COVID-19 patients. It seems that CAFDs have better absorption and good safety profiles as many studies pointed out the better absorption of CAFDs and CAFDs are important constituent of dietary foods. However, it would be worthwhile to conduct pharmacological studies to determine whether the bioavailability of CAFDs is good enough or it is better to administer in combinations. Once we

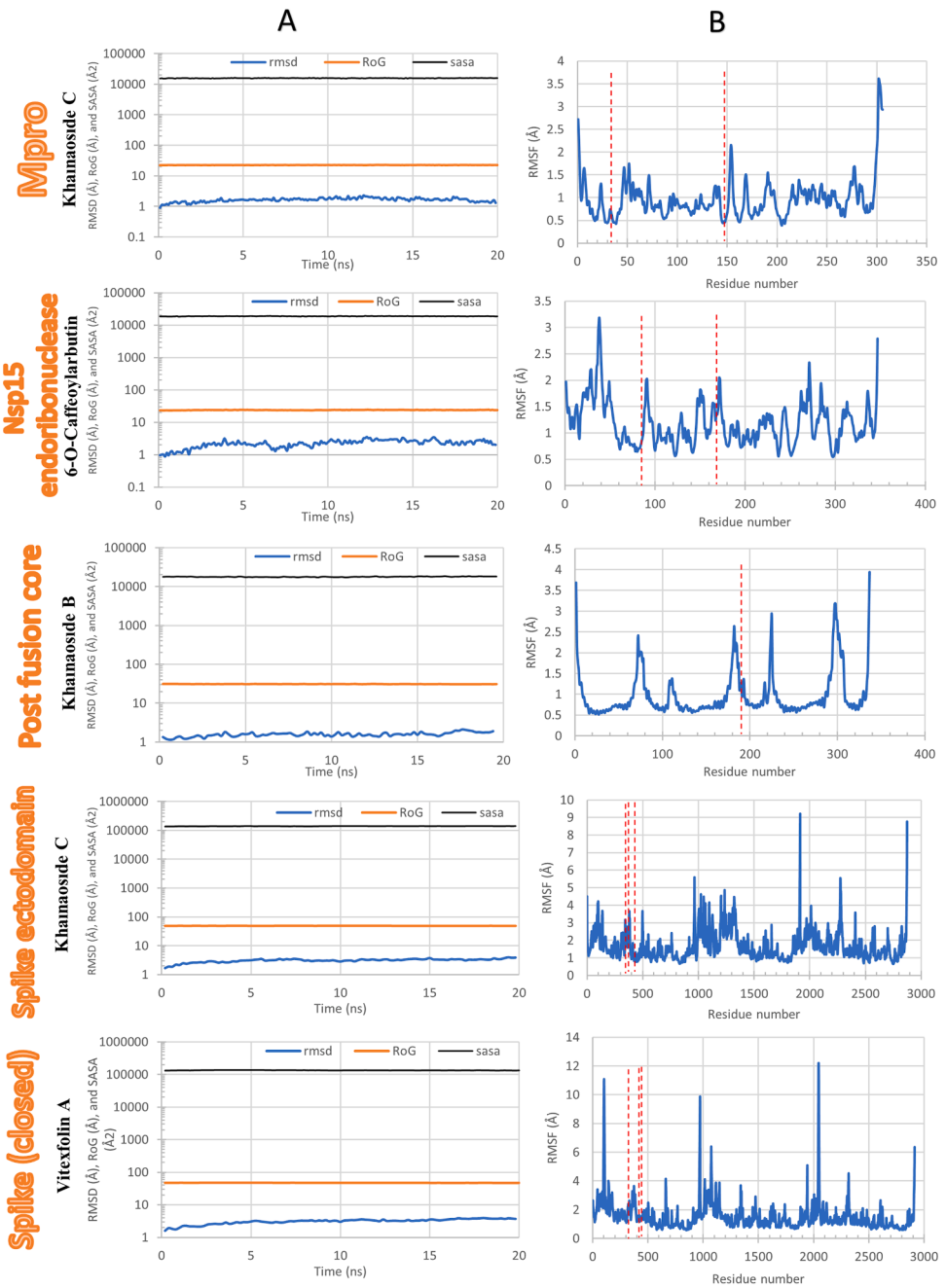

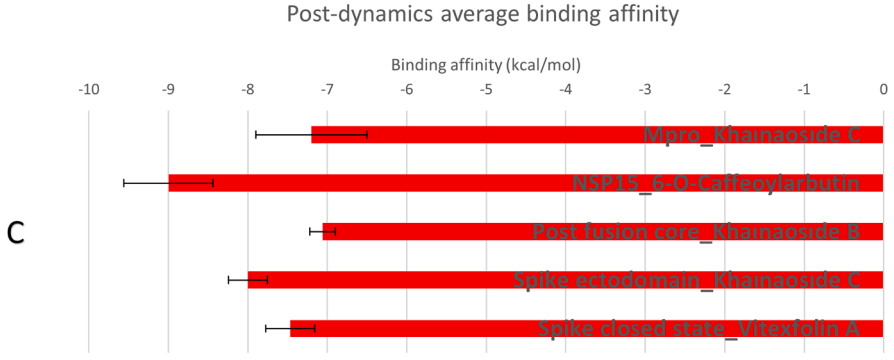

C

Fig. 9. Post-dynamics analysis: (A) Root Mean Square Deviation (RMSD) (blue line), Radius of Gyration (RoG) (orange line), and surface accessible surface area (SASA) (gray line) for the best complex for each viral protein during 20 ns MDS run. (B) Per-residue Root Mean Square Fluctuation (RMSF) for the same complexes with dashed lines represents the active residues. (C) Post-dynamics average binding energies (in kcal/mol) calculated for the complexes using AutoDock Vina. Error bars represent the standard deviations.

understand the best way to deal with the CAFDs, it will be a reasonable starting point for therapeutic interventions based on the pharmacokinetic and pharmacodynamic studies on CAFDs. Despite excitement about CAFD's potential from antiviral and anti-inflammatory researches, there is an urgent and timely need to fill the room of knowledge for validation of CAFDs potential against COVID-19.

Acknowledgment

Shaheen supercomputer of King Abdullah University of Science and Technology (KAUST) is used to perform the MDS study (under the project number k1482). We thank Dr. Bahaa Mostafa for using his computational power unit during the analysis of the MDS data.

References

Abu-Reidah, I.M., Contreras, M.M., Arraez-Roman, D., Segura-Carretero, A., Fernandez-Gutierrez, A., 2013. Reversed-phase ultra-high-performance liquid chromatography coupled to electrospray ionization-quadrupole-time-of-flight mass spectrometry as a powerful tool for metabolic profiling of vegetables: Lactuca sativa as an example of its application. J. Chromatogr. A 1313, 212–227.

Adem, S., Eyupoglua, V., Sarfraz, I., Rasul, A., 2020. Identification of potent COVID-19 main protease (Mpro) inhibitors from natural polyphenols: an in silico strategy unveils a hope against CORONA.

Amoretti, M., Amsler, C., Bonomi, G., Bouchta, A., Bowe, P., Carraro, C., Cesar, C.L., Charlton, M., Collier, M.J., Doser, M., Filippini, V., Fine, K.S., Fontana, A., Fujiwara, M.C., Funakoshi, R., Genova, P., Hangst, J.S., Hayano, R.S., Holzscheiter, M.H., Jorgensen, L.V., Lagomarsino, V., Landua, R., Lindelof, D., Lodi Rizzini, E., Macri, M., Madsen, N., Manuzio, G., Marchesotti, M., Montagna, P., Pruys, H., Regenfus, C., Riedler, P., Rochet, J., Rotondi, A., Rouleau, G., Testera, G., Variola, A., Watson, T.L., van der Werf, D.P., Collaboration, A., 2002. Production and detection of cold antihydrogen atoms. Nature 419, 456–459.

Buzon, V., Natrajan, G., Schibli, D., Campelo, F., Kozlov, M.M., Weissenhorn, W., 2010. Crystal structure of HIV-1 gp41 including both fusion peptide and membrane proximal external regions. PLoS Pathog. 6, e1000880.

Daina, A., Michielin, O., Zoete, V., 2017. SwissADME: a free web tool to evaluate pharmacokinetics, drug-likeness and medicinal chemistry friendliness of small molecules. Sci. Rep. 7, 42717.

Dong, Z., Lu, X., Tong, X., Dong, Y., Tang, L., Liu, M., 2017. Forsythiae fructus: a review on its phytochemistry, quality control, pharmacology and pharmacokinetics. molecules 22.

Dos Santos, C.N., Menezes, R., Stewart, D., 2018. Polyphenols as new leads in drug discovery: biological activity and mechanisms. Curr. Pharm. Des. 24, 2041–2042.

Du, R.H., Liang, L.R., Yang, C.Q., Wang, W., Cao, T.Z., Li, M., Guo, G.Y., Du, J., Zheng, C. L., Zhu, Q., Hu, M., Li, X.Y., Peng, P., Shi, H.Z., 2020. Predictors of mortality for patients with COVID-19 pneumonia caused by SARS-CoV-2: a prospective cohort study. Eur. Respir. J.

Guo, Y.R., Cao, Q.D., Hong, Z.S., Tan, Y.Y., Chen, S.D., Jin, H.J., Tan, K.S., Wang, D.Y., Yan, Y., 2020. The origin, transmission and clinical therapies on coronavirus disease 2019 (COVID-19) outbreak - an update on the status. Military Med. Res. 7, 11.

Huang, J., MacKerell Jr., A.D., 2013. CHARMM36 all-atom additive protein force field: validation based on comparison to NMR data. J. Comput. Chem. 34, 2135–2145.

Humphrey, W., Dalke, A., Schulten, K., 1996. VMD: visual molecular dynamics. Journal of molecular graphics 14. J. Mol. Graph. 14, 33–38.

Hussain, M., Jabeen, N., Raza, F., Shabbir, S., Baig, A.A., Amanullah, A., Aziz, B., 2020. Structural variations in human ACE2 may influence its binding with SARS-CoV-2 spike protein. J.Med. Virol.

Jasso-Miranda, C., Herrera-Camacho, I., Flores-Mendoza, L.K., Dominguez, F., Vallejo-Ruiz, V., Sanchez-Burgos, G.G., Pando-Robles, V., Santos-Lopez, G., Reyes-Leyva, J., 2019. Antiviral and immunomodulatory effects of polyphenols on macrophages infected with dengue virus serotypes 2 and 3 enhanced or not with antibodies. Infect. Drug Resist. 12, 1833–1852.

Jin, H.G., Kim, A.R., Ko, H.J., Lee, S.K., Woo, E.R., 2014. Three new lignan glycosides with IL-6 inhibitory activity from Akebia quinata. Chem. Pharm. Bull. 62, 288–293.

Jin, Z., Du, X., Xu, Y., Deng, Y., Liu, M., Zhao, Y., Zhang, B., Li, X., Zhang, L., Peng, C., Duan, Y., Yu, J., Wang, L., Yang, K., Liu, F., Jiang, R., Yang, X., You, T., Liu, X., Yang, X., Bai, F., Liu, H., Liu, X., Guddat, L.W., Xu, W., Xiao, G., Qin, C., Shi, Z., Jiang, H., Rao, Z., Yang, H., 2020. Structure of M(pro) from SARS-CoV-2 and discovery of its inhibitors. Nature 582, 289–293.

Jing, J., Chan, C.O., Xu, L., Jin, D., Cao, X., Mok, D.K., Parekh, H.S., Chen, S., 2011. Development of an in-line HPLC fingerprint ion-trap mass spectrometric method for identification and quality control of Radix Scrophulariae. J. Pharm. Biomed. Anal. 56, 830–835.

Jo, S., Kim, T., Iyer, V.G., Im, W., 2008. CHARMM-GUI: a web-based graphical user interface for CHARMM. J. Comput. Chem. 29, 1859–1865.

Khan, M.F., Khan, M.A., Khan, Z.A., Ahamad, T., Ansari, W.A., 2020. Identification of dietary molecules as therapeutic agents to combat COVID-19 using molecular docking studies.

Kim, H.J., Yu, Y.G., Park, H., Lee, Y.S., 2002. HIV gp41 binding phenolic components from Fraxinus sieboldiana var. Angustata. Planta Med. 68, 1034–1036.

Kim, Y., Jedrzejczak, R., Maltseva, N.I., Endres, M., Godzik, A., Michalskaa, K., Joachimiak, A., 2020a. Crystal structure of Nsp15 endoribonuclease NendoU from SARS-CoV-2.

Kim, Y., Jedrzejczak, R., Maltseva, N.I., Wilamowski, M., Endres, M., Godzik, A., Michalska, K., Joachimiak, A., 2020b. Crystal structure of Nsp15 endoribonuclease NendoU from SARS-CoV-2. Protein Sci.: A Publ. Protein Soc. 29, 1596–1605.

Lalani, S., Poh, C.L., 2020. Flavonoids as antiviral agents for enterovirus A71 (EV-A71). Viruses 12.

Langland, J., Jacobs, B., Wagner, C.E., Ruiz, G., Cahill, T.M., 2018. Antiviral activity of metal chelates of caffeic acid and similar compounds towards herpes simplex, VSV-Ebola pseudotyped and vaccinia viruses. Antiviral Res. 160, 143–150.

Li, Z.J., Shen, X.Y., Hou, C.L., 2016. Fungal endophytes of South China blueberry (Vaccinium dunalianum var. urophyllum). Lett. Appl. Microbiol. 63, 482–487.

Lin, Z., Neamati, N., Zhao, H., Kiryu, Y., Turpin, J.A., Aberham, C., Strebel, K., Kohn, K., Witvrouw, M., Pannecouque, C., Debyser, Z., De Clercq, E., Rice, W.G., Pommier, Y., Burke Jr., T.R., 1999. Chicoric acid analogues as HIV-1 integrase inhibitors. J. Med. Chem. 42, 1401–1414.

Liu, X., Wang, X.J., 2020. Potential inhibitors against 2019-nCoV coronavirus M protease from clinically approved medicines. J. Genet. Genom. = Yi chuan xue bao 47, 119–121.

Lu, R., Zhao, X., Li, J., Niu, P., Yang, B., Wu, H., Wang, W., Song, H., Huang, B., Zhu, N., Bi, Y., Ma, X., Zhan, F., Wang, L., Hu, T., Zhou, H., Hu, Z., Zhou, W., Zhao, L., Chen, J., Meng, Y., Wang, J., Lin, Y., Yuan, J., Xie, Z., Ma, J., Liu, W.J., Wang, D., Xu, W., Holmes, E.C., Gao, G.F., Wu, G., Chen, W., Shi, W., Tan, W., 2020. Genomic characterisation and epidemiology of 2019 novel coronavirus: implications for virus origins and receptor binding. Lancet 395, 565–574.

Luecha, P., Umehara, K., Miyase, T., Noguchi, H., 2009. Antiestrogenic constituents of the Thai medicinal plants Capparis flavicans and Vitex glabrata. J. Nat. Prod. 72, 1954–1959.

Luo, X.L., Li, N., Xu, M., Zhu, H.T., He, P., Ding, Y., Zhao, P., Zhang, Y.J., 2015. HPLC simultaneous determination of arbutin, chlorogenic acid and 6′-O-caffeoylarbutin in different parts of Vaccinium dunalianum Wight. Nat. Prod. Res. 29, 1963–1965.

Magnani, C., Isaac, V., Corrêa, M.A., Salgado, H., 2014. Caffeic acid: a review of its potential use in medications and cosmetics. Anal. Methods 6, 3203.

Mark, P., Nilsson, L., 2001. Structure and Dynamics of the TIP3P, SPC, and SPC/E Water Models at 298 K. J. Phys. Chem. 105, 9954–9960.

Morris, G.M., Huey, R., Lindstrom, W., Sanner, M.F., Belew, R.K., Goodsell, D.S., Olson, A.J., 2009. AutoDock4 and AutoDockTools4: automated docking with selective receptor flexibility. J. Comput. Chem. 30, 2785–2791.

Ogawa, M., Shirasago, Y., Ando, S., Shimojima, M., Saijo, M., Fukasawa, M., 2018. Caffeic acid, a coffee-related organic acid, inhibits infection by severe fever with thrombocytopenia syndrome virus in vitro. J. Infect. Chemother.: Off. J. Jpn Soc. Chemother. 24, 597–601.

Okuyama, E., Fujimori, S., Yamazaki, M., Deyama, T., 1998. Pharmacologically active components of viticis fructus (Vitex rotundifolia). II. The components having analgesic effects. Chem. Pharm. Bull. 46, 655–662.

Peng, Y., Sun, Q., Park, Y., 2019. The bioactive effects of chicoric acid as a functional food ingredient. J. Med. Food 22, 645–652.

Pettersen, E.F., Goddard, T.D., Huang, C.C., Couch, G.S., Greenblatt, D.M., Meng, E.C., Ferrin, T.E., 2004. UCSF Chimera–a visualization system for exploratory research and analysis. J. Comput. Chem. 25, 1605–1612.

Phillips, J.C., Braun, R., Wang, W., Gumbart, J., Tajkhorshid, E., Villa, E., Chipot, C., Skeel, R.D., Kale, L., Schulten, K., 2005. Scalable molecular dynamics with NAMD. J. Comput. Chem. 26, 1781–1802.

Pluymers, W., Neamati, N., Pannecouque, C., Fikkert, V., Marchand, C., Burke Jr., T.R., Pommier, Y., Schols, D., De Clercq, E., Debyser, Z., Witvrouw, M., 2000. Viral entry as the primary target for the anti-HIV activity of chicoric acid and its tetra-acetyl esters. Mol. Pharmacol. 58, 641–648.

Somtimuang, C., Olatunji, O.J., Ovatlarnporn, C., 2018. Evaluation of in vitro alpha-amylase and alpha-glucosidase inhibitory potentials of 14 medicinal plants constituted in Thai folk antidiabetic formularies. Chem. Biodivers. 15, e1800025.

Sun, Z., Chen, J., Ma, J., Jiang, Y., Wang, M., Ren, G., Chen, F., 2012. Cynarin-rich sunflower (Helianthus annuus) sprouts possess both antiglycative and antioxidant activities. J. Agric. Food Chem. 60, 3260–3265.

Trott, O., Olson, A.J., 2010. AutoDock Vina: improving the speed and accuracy of docking with a new scoring function, efficient optimization, and multithreading. J. Comput. Chem. 31, 455–461.

Utsunomiya, H., Ichinose, M., Ikeda, K., Uozaki, M., Morishita, J., Kuwahara, T., Koyama, A.H., Yamasaki, H., 2014. Inhibition by caffeic acid of the influenza A virus multiplication in vitro. Int. J. Mol. Med. 34, 1020–1024.

Vazquez-Calvo, A., Jimenez de Oya, N., Martin-Acebes, M.A., Garcia-Moruno, E., Saiz, J. C., 2017. Antiviral properties of the natural polyphenols delphinidin and epigallocatechin gallate against the Flaviviruses West Nile Virus, Zika Virus, and Dengue Virus. Front. Microbiol. 8, 1314.

Walls, A.C., Park, Y.J., Tortorici, M.A., Wall, A., McGuire, A.T., Veesler, D., 2020a. Structure, function, and antigenicity of the SARS-CoV-2 spike glycoprotein. Cell 181, 281–292 e286.

Walls, A.C., Park, Y.J., Tortorici, M.A., Wall, A., McGuire, A.T., Veesler, D., 2020b. Structure, function, and antigenicity of the SARS-CoV-2 spike glycoprotein. Cell.

Wang, F.N., Ma, Z.Q., Liu, Y., Guo, Y.Z., Gu, Z.W., 2009. New phenylethanoid glycosides from the fruits of forsythia suspense (thunb.) vahl. Molecules 14, 1324–1331.

Wang, H., Zhao, W., Choomuenwai, V., Andrews, K.T., Quinn, R.J., Feng, Y., 2013. Chemical investigation of an antimalarial Chinese medicinal herb Picrorhiza scrophulariiflora. Bioorg. Med. Chem. Lett. 23, 5915–5918.

Wang, X., Yu, N., Peng, H., Hu, Z., Sun, Y., Zhu, X., Jiang, L., Xiong, H., 2019. The profiling of bioactives in Akebia trifoliata pericarp and metabolites, bioavailability

and in vivo anti-inflammatory activities in DSS-induced colitis mice. Food & Funct. 10, 3977–3991.
Wu, F., Zhao, S., Yu, B., Chen, Y.M., Wang, W., Song, Z.G., Hu, Y., Tao, Z.W., Tian, J.H., Pei, Y.Y., Yuan, M.L., Zhang, Y.L., Dai, F.H., Liu, Y., Wang, Q.M., Zheng, J.J., Xu, L., Holmes, E.C., Zhang, Y.Z., 2020. A new coronavirus associated with human respiratory disease in China. Nature 579, 265–269.
Xia, S., Liu, M., Wang, C., Xu, W., Lan, Q., Feng, S., Qi, F., Bao, L., Du, L., Liu, S., Qin, C., Sun, F., Shi, Z., Zhu, Y., Jiang, S., Lu, L., 2020. Inhibition of SARS-CoV-2 (previously 2019-nCoV) infection by a highly potent pan-coronavirus fusion inhibitor targeting its spike protein that harbors a high capacity to mediate membrane fusion. Cell Res. 30, 343–355.
Zhang, H.L., Dai, L.H., Wu, Y.H., Yu, X.P., Zhang, Y.Y., Guan, R.F., Liu, T., Zhao, J., 2014. Evaluation of hepatocyteprotective and anti-hepatitis B virus properties of Cichoric acid from Cichorium intybus leaves in cell culture. Biol. Pharm. Bull. 37, 1214–1220.
Zhao, Y.H., Abraham, M.H., Le, J., Hersey, A., Luscombe, C.N., Beck, G., Sherborne, B., Cooper, I., 2002. Rate-limited steps of human oral absorption and QSAR studies. Pharm. Res. 19, 1446–1457.
Zhu, N., Zhang, D., Wang, W., Li, X., Yang, B., Song, J., Zhao, X., Huang, B., Shi, W., Lu, R., Niu, P., Zhan, F., Ma, X., Wang, D., Xu, W., Wu, G., Gao, G.F., Tan, W., China Novel Coronavirus, I., Research, T., 2020. A novel coronavirus from patients with pneumonia in China, 2019. N. Engl. J. Med. 382, 727–733.